INTERNATIONAL JOURNAL FOR NUMERICAL METHODS IN BIOMEDICAL ENGINEERING
Int. J. Numer. Meth. Biomed. Engng. 2014; **30**:1372–1386
Published online 3 August 2014 in Wiley Online Library (wileyonlinelibrary.com). DOI: 10.1002/cnm.2662

Human heart conjugate cooling simulation: Unsteady thermo-fluid-stress analysis

Abas Abdoli[1], George S. Dulikravich[1,*,†], Chandrajit Bajaj[2], David F. Stowe[3] and M. Salik Jahania[4]

[1]*Department of Mechanical and Materials Engineering, MAIDROC Laboratory, Florida International University, Miami, FL 33174*
[2]*Department of Computer Sciences, Computational Visualization Center, Institute of Computational Engineering and Sciences, University of Texas at Austin, Austin, TX 78712*
[3]*Departments of Anesthesiology and Physiology, Cardiovascular Research Center, Medical College of Wisconsin, Research Service, Veterans Affairs Medical Center, Milwaukee, WI 53295*
[4]*Department of Surgery, Division of Cardiothoracic Surgery, School of Medicine, Wayne State University, Detroit, MI 48202*

SUMMARY

The main objective of this work was to demonstrate computationally that realistic human hearts can be cooled much faster by performing conjugate heat transfer consisting of pumping a cold liquid through the cardiac chambers and major veins while keeping the heart submerged in cold gelatin filling a cooling container. The human heart geometry used for simulations was obtained from three-dimensional, high resolution CT-angio scans. Two fluid flow domains for the right (pulmonic) and left (systemic) heart circulations, and two solid domains for the heart tissue and gelatin solution were defined for multi-domain numerical simulation. Detailed unsteady temperature fields within the heart tissue were calculated during the conjugate cooling process. A linear thermoelasticity analysis was performed to assess the stresses applied on the heart due to the coolant fluid shear and normal forces and to examine the thermal stress caused by temperature variation inside the heart. It was demonstrated that a conjugate cooling effort with coolant temperature at +4°C is capable of reducing the average heart temperature from +37°C to +8°C in 25 minutes for cases in which the coolant was steadily pumped only through major heart inlet veins and cavities. Copyright © 2014 John Wiley & Sons, Ltd.

Received 4 January 2014; Revised 25 April 2014; Accepted 6 July 2014

KEY WORDS: heart simulation; organ preservation; transplantation; heart cooling; conjugate heat transfer; cryopreservation

1. INTRODUCTION

The main problem in transplantation organ delivery is the relatively short time that organs can survive from the moment of their harvesting to the moment of their surgical implantation. Currently, the time limit for an explanted human heart to remain viable is only 4 hours when the heart is kept submerged in a saline solution at a temperature close to that of freezing water [1]. In most cases, the donor and the recipient of the compatible heart are at vastly different geographic locations. This means that the current 4 hours limitation must cover transportation from the site of harvesting to the nearest airport, flight time to the airport nearest to the recipient's location, and travel time from that airport to the hospital where the recipient is located. In practice, this leaves at most 2.5 hours for air transportation of the heart, which is insufficient to cover even half of the territory of the United

*Correspondence to: George S. Dulikravich, Department of Mechanical and Materials Engineering, MAIDROC Laboratory, Florida International University, Miami, FL 33174.
†E-mail: dulikrav@fiu.edu

States. The ultimate objective of this research is to demonstrate a feasibility of a heart perfusion concept to extend the viability of the transplant heart to at least 7 hours. This would provide up to 5.5 hours for air transport, thus enabling heart transplantations anywhere in the United States. As part of achieving this goal, the just explanted heart should be brought to a just-above tissue freezing temperature as uniformly and as quickly as possible.

Cold preservation takes advantage of the profound effect of decreasing cell temperature to decrease the cell metabolic rate to avert cell death. The well-known "Q_{10} law" [2] states that for every 10°C reduction in tissue temperature there is a corresponding reduction in cell metabolism equal to the constant Q_{10}. The law is written as

$$\frac{q_m}{q_{m\,0}} = (\mathrm{Q}_{10})^{[(T-T_0)/10]} \tag{1}$$

where T is temperature in degrees Celsius and q_m is the cell metabolic rate. Values for Q_{10} range from 2.0 to 3.0 and are cited in the physiology literature [2]. For example, assuming a mid-range value, say $Q_{10} = 2.5$, it can be observed that reducing temperature from +37°C to +27°C reduces the metabolic rate by a factor of 2.5. Reducing temperature to +4°C reduces the metabolic rate by 95%. As a result of reducing the cell metabolic rate, oxygen and glucose consumption and carbon dioxide production are decreased as well [3]. Thus, the cell damage due to lack of oxygen will be decreased [4]. For example, Stowe *et al*. [5] showed that stopping tissue perfusion and cooling isolated guinea pig hearts to +3.4°C for 6 hours resulted in a return of left ventricular pressure of up to 81% of that before cooling. Jahania *et al*. [6] described the protective strategy and principles for using hypothermia in heart preservation.

Numerical studies in this field are very challenging due to the geometric complexity of the heart and lack of certain experimental data for the non-isotropic properties of its tissue. Dulikravich [7] demonstrated, in the case of two dimensions, that it is possible to maintain specified cooling rates at any point of the cooled object by varying container wall temperature distribution. Dennis and Dulikravich [8] used 3-D spectral finite elements method to simulate unsteady temperature and thermal stress fields during freezing of an idealized canine kidney submerged in gelatin without perfusion. Using finite elements method coupled with an optimization algorithm they also optimized time-varying temperatures and heat fluxes to be used on the surface of a spherical freezing container and suggested optimizing the internal perfusion temperature of the organ during the cooling process. Sterk and Trobec [9] simulated a 3-D heart model submerged inside the cooling liquid without perfusion. They used an explicit finite difference method to solve Navier-Stokes equations to account for thermal buoyancy flow inside the cooling liquid bath, but not inside the heart.

In the present computational study, a combined 3-D thermo-fluid-stress analysis was performed to simulate the temperature distribution within the human heart during a cooling process which applies a steadily flowing cooling fluid for internal cooling and a cooling gel for external cooling.

2. DESIGN AND FORMULATIONS

A conjugate cooling protocol for human heart preservation was presented. In this protocol, the realistic human heart was computationally created and externally cooled by immersing it in cold gelatin contained in a defined cooling container. At the same time, the heart interior surfaces (chambers and inlet and outlet vessels) were continuously perfused with a cold liquid provided by a pump.

The blood circulatory system of the heart consists of the systemic (left) and pulmonary (right) circulations [10]. Ranges in the velocity of blood flow in the major inflow and outflow vessels of the heart (Table I) indicate that maximal blood flow ejection velocity is in the aorta, whereas the

Table I. Velocity of blood flow.

Major Blood Vessel	**Inlet/Outlet**	**Velocity (cm/s) [reference]**
Superior Vena Cava	Inlet	10-35 [11]
Inferior Vena Cava	Inlet	30-45 [11]
Aorta	Outlet	108-120 [12]

DOI: 10.1002/cnm

superior vena cava has a minimal and smaller inlet velocity compared to the inferior vena cava. The UW solution was simulated as pumped steadily in the heart by considering the natural direction of blood flow circulation in order to prevent damaging the heart valves.

The geometry of the human heart is a major challenge for undertaking this thermal-fluid-stress analysis. Bajaj's team [13, 14] performed multi-component heart reconstruction, segmentation and meshing from volumetric imaging. They applied a distant function technique in geometry modeling to generate a 3-D finite-element and boundary element human heart mesh from high resolution CT-angio imaging data. This geometry was used in the present research.

This model does not include the coronary circulation; that is, this internal heart cooling system consisted of coolant pumped through the major vessels and heart chambers. The multi-physical components of this computational analysis required three separate domains; inside the heart (chambers), the heart tissue itself, and outside the heart.

Figure 1 demonstrates different domain surfaces in different colors. A hexahedra (Figure 2a) of 214 mm in length, 212 mm in width and 282 mm in height, with 4 inlets and 4 outlets was computationally designed as the heart-cooling container. Figure 2b shows the designed connections and caps for steadily pumping coolant through the pulmonic and systemic vessels.

For each of the heart circulatory systems, two inlets and two outlets were incorporated to pump the coolant through the heart chambers as shown in figures 2c and 2d. For the right (pulmonic) heart circulation, the inferior vena cava and superior vena cava were the two flow inlets and one of the right pulmonary arteries and one of the left pulmonary arteries were the two flow outlets. For the left (systemic) heart

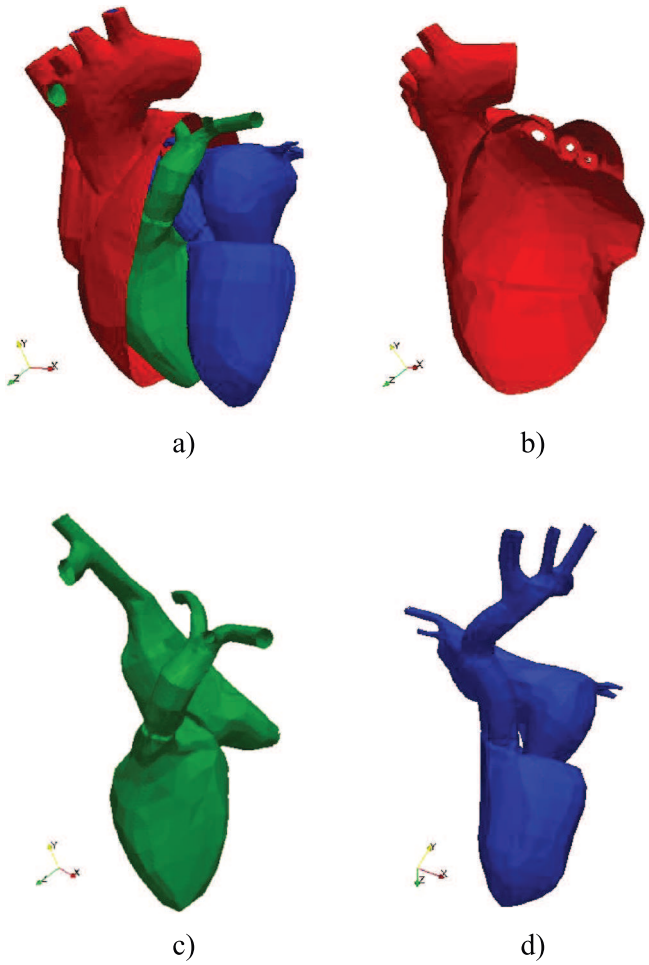

Figure 1. Heart surfaces: a) all surfaces, b) outermost surfaces, c) heart pulmonary circulation domain surfaces, and d) heart systemic circulation domain surfaces.

DOI: 10.1002/cnm

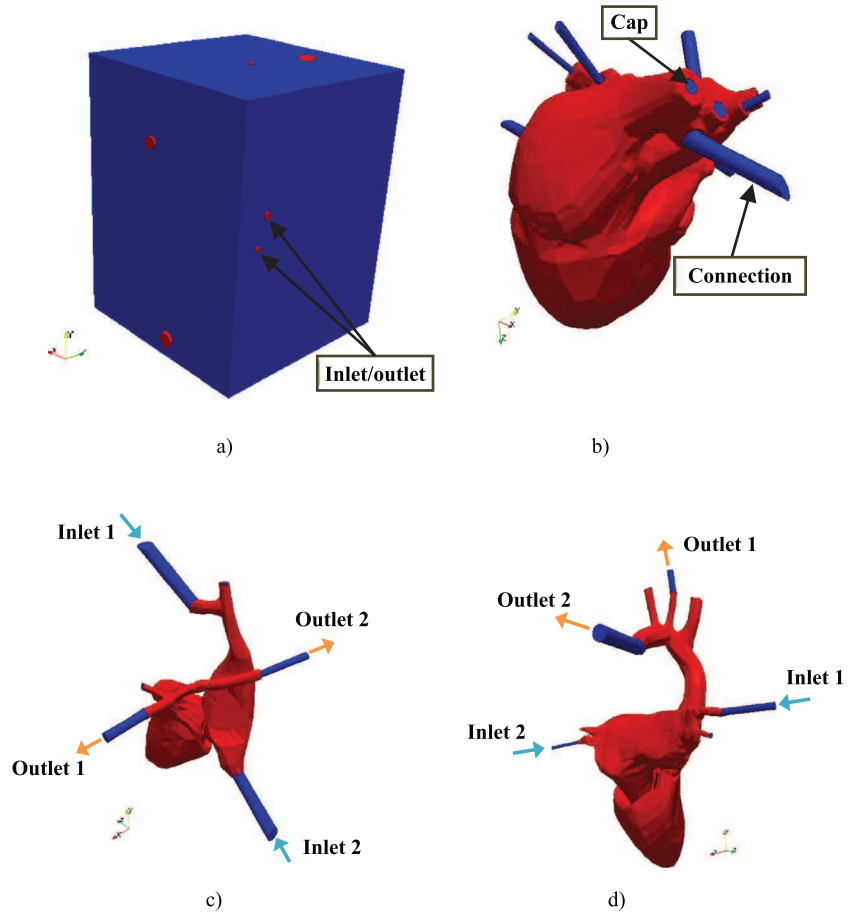

Figure 2. Cooling system: a) cooling container, b) connections and caps, c) circulation directions for the right (pulmonic) heart, and d) circulation directions for the left (systemic) heart.

circulation, one of the left pulmonary veins and one of the right pulmonary veins were the two flow inlets, and the aorta plus one of its cephalad branches (left common carotid artery) were the two flow outlets.

As these figures illustrate, for the simulation the coolant was pumped into the heart chambers in the same directions as that in an intact heart and circulatory system. This allowed for the cooling solution to flow through chambers with the heart valves promoting forward flow and preventing backward flow, as occurs naturally. At the same time, the heart was submersed in a cold gelatin to allow for pure conduction cooling applied from outside the heart. Heat conduction affords the benefit of having different cooling rates locally in the heart when applying different temperatures on the walls of the cooling container.

The different viscosity, specific heat, heat conductivity, and density properties of the heart and cooling fluid and gelatin required the modeling analysis to have different domains for solids and fluids. The University of Wisconsin (UW) solution was chosen as the liquid to pump through the chambers. UW solution remains as the standard for organ preservation [15] despite the development of other cooling solutions that are superior in some aspects. This coolant was considered as a Newtonian fluid and was modeled by using the Navier-Stokes equations for incompressible viscous fluid flow satisfying conservation of mass, linear momentum and energy. The thermophysical

Table II. Thermophysical properties.

Material	**Density, ρ** ($kg\ m^{-3}$)	**Specific Heat, C** ($J\ kg^{-1}\ K^{-1}$)	**Heat Conductivity, k** ($W\ m^{-1}\ K^{-1}$)	**Viscosity, μ** ($kg\ m^{-1}\ s^{-1}$)
UW solution [16]	1025	4180	0.6	0.0037
Heart tissue [17]	1060	3716.98	0.586	-

DOI: 10.1002/cnm

properties of the UW solution and heart are shown in Table II. The thermal properties of gelatin were assumed to be the same as for the UW solution.

There is no available data for the critical Reynolds number inside the heart. Kisslo and Adams [18] demonstrated that the blood flow inside the heart, great vessels and most of the cardiovascular system is normally laminar. In the present analysis, the inlet vein flow velocity for the right heart pulmonary circulation was assumed to be 1.0 m/s, and 0.4 m/s for the left heart systemic circulation. Therefore, the values of Reynolds numbers at the inlets, with consideration of their diameters, were 1662 and 1773 for the right heart pulmonary circulation and 1330 and 665 for the left heart systemic circulation. Stein and Sabbah [19] studied the turbulent blood flow in the ascending aorta of humans with normal and diseased aortic valves. They reported that the critical Reynolds number in smooth, straight pipes, which is 2300, is also an acceptable criterion for the blood flow pattern inside the aorta. They mentioned that for Reynolds numbers below 2300, even strong disturbances do not cause the flow to become turbulent. The turbulent flow in the aorta is mainly due to the aortic valve opening and closing and the pulsatile flow by muscle contraction. However, in the present model the flow was uniform through open valves. In the present study, considering these very low Reynolds numbers, static-open position of valves and by taking into account Kisslo, Adams, Stein and Sabbah's observations, the flow of cooling fluid inside the heart chambers and vessels was assumed to be laminar.

The OpenFOAM software platform was used for simulations [20] of thermo-fluid fields governed by Navier-Stokes equations for unsteady, three-dimensional, laminar, Newtonian fluid flow with convective heat transfer at the fluid solid interfaces. OpenFOAM applies the PISO (Pressure Implicit with Splitting of Operators) algorithm [21] for the pressure–velocity transient problems. This algorithm allows for more than one pressure-velocity correction. Another correction can be applied to account for the non-orthogonality of the computational grid. For the solid domains, only energy balance was applied, known as the transient heat conduction equation.

Unsteady stress-deformation analysis was performed simultaneously with fluid flow analysis and heat transfer analysis for the simulated heart during the cooling process. The main objectives of the stress analysis were to investigate thermal stresses and internal shear stresses applied by pumping the cooling fluid from the vessels to the chambers. The pressure inside the resting heart during cooling is less than the diastolic pressure of the beating heart. Because the heart will not be beating and the cooling process will be continuous (constant flow), it is acceptable to assume there would be little deformation of the heart chambers or vessels during the cooling process. The classical theory of unsteady three-dimensional linear thermoelasticity was used to evaluate stresses and deformations throughout heart tissue. The OpenFOAM stress analysis solver (solidDisplacementFoam) was applied for solving these equations. This solver is a transient, segregated, finite-volume solver of linear-elastic, small-strain deformation. It also includes the thermal stresses. Heart tissue and cooling gelatin were considered as isotropic solid materials [22]. Heart has different types of tissues with very complex behaviors, especially in dynamic situations when large deformations are involved. The main objective of stress analysis in this study was to give an initial understanding of stress distributions within a static heart during cooling process. The mechanical properties of heart that were used are given in Table III.

A fully three-dimensional unsteady conjugate heat transfer analysis was performed by solving the governing equations for fluid and solid domains. The main benefit of performing the conjugate heat transfer analysis was that interface temperature distributions and heat flux distributions could be captured iteratively and accurately.

In the present work, a numerical procedure for coupling fluid and solid domains was applied that utilizes separate solution matrices, separate mesh discretizations, and separate numerical algorithms for fluid and solid domains [27]. A first order implicit Euler scheme was applied for time discretization. Solvers for each domain were placed inside a loop to achieve the coupled convergence through a

Table III. Mechanical properties.

Material	Young's Elastic Modulus (kPa)	Ultimate Tensile Stress (kPa)	Poisson's Ratio	Thermal Expansion Coefficient ($°C^{-1}$)
Cardiac Muscle	80 [23]	110 [23, 24]	0.4 [25]	0.0003 [26]

DOI: 10.1002/cnm

Table IV. Grid cells for different computational domains.

Domain	Number of grid cells
Heart pulmonary circulation	~ 700,000
Heart systemic circulation	~ 900,000
Heart	~ 1,200,000
Gelatin	~ 1,400,000

global iterative process. Multi-region, three-dimensional, unsteady conjugate heat transfer OpenFOAM solver (chtMultiRegionFoam) was applied for simulations. The chtMultiRegionFoam is a parallel solver that has been validated by different researchers [28]. The hexahedral mesh was generated for each domain using the OpenFOAM snappyHexMesh [20] method. The snappyHexMesh is able to create a robust and fast meshing for complex geometries. In this method, geometry can be defined as stl (stereolithography) file format, which is desirable in biomedical applications. Table IV shows the number of computational grid cells used in each domain. The total number of grid cells for all domains was 4,200,000.

3. RESULTS AND DISCUSSIONS

In this section results of two different cooling scenarios are presented. In the first scenario, the heart was cooled by pure conduction using gelatin from the outside and with no liquid cooling from the inside. In the second scenario, convection liquid cooling from the inside and conduction gelatin cooling from outside were implemented to examine conjugate effect in enhancing heat transfer from the heart.

3.1. Cooling with gelatin only

For this simulation, a multi-domain unsteady conduction heat transfer equation was solved for the heart tissue and the outside gelatin. Temperature boundary conditions for the cooling container walls are given in Table V. Each wall had a constant value for temperature. The minimum and maximum wall temperatures were set at -1°C and +1°C, respectively. The minimum wall temperature could be less than -1°C, but the reason for choosing -1°C as the minimum temperature was to avoid cooling of the heart below +4°C, which might damage the heart cells if pure water domains were allowed to form ice crystals. Two wall temperatures, one set to 0°C and one set to +1°C (Table V) were used to investigate the influence of different wall temperatures on differential cooling of the heart. The initial temperature of gelatin was assumed to be +4°C. The initial temperature of the heart was assumed to be +37°C.

Heat transfer analysis was performed for a 1500 s period. It was assumed that the major temperature reduction should occur within this time interval in order to cool the heart to a steady low temperature before its long range transportation to the implantation site. A workstation computer with the Ubuntu 13.10 Linux OS was used for this simulation. Thermal simulation was run on 4 cores of an Intel Core i7, 3.4 GHz, Six Core with 64 GB memory. Total computing time was 2532 s.

Figure 3a shows the temperature distribution in a cutaway view for a constant range of color bar from -1°C to +37°C. As this figure illustrates, there was a very large size higher temperature region remaining in the middle of the heart after 1500 s.

Figure 3b shows a slight reduction in the maximum temperature of the heart to +36.7°C after 1500 s of cooling with gelatin only. Similarly, the average volumetric temperature of the heart tissue was reduced to only +21°C after 1500 s. In this computational study, average volumetric temperature refers to the average temperature of all computational cells by considering their volumes. This suggests that pure heat conduction cooling with gelatin from the outside of the heart and no liquid cooling from inside the heart was not capable of removing sufficient amount of heat within the target time interval of 1500 s.

Table V. Boundary conditions for cooling container walls.

Container Wall at	X_{max}	X_{min}	Y_{max}	Y_{min}	Z_{max}	Z_{min}
Temperature	0°C	-1°C	-1°C	-1°C	0°C	+1°C

DOI: 10.1002/cnm

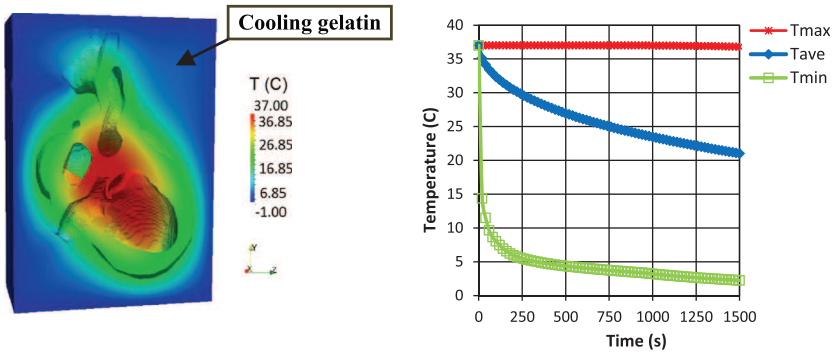

a) b)

Figure 3. Temperature variation (cooling with gelatin only): a) inside the heart and gelatin with constant color legend (cut-away view) at 300 s, and b) maximum, minimum and average volumetric temperatures of the heart *vs*. time.

3.2. Cooling with gelatin and liquid

We considered that there are two separate fluid domains, one for the right heart pulmonary circulation, and one for the left heart systemic circulation. Table VI shows the boundary conditions applied for these two domains. Considering the maximal averaged velocity of blood flow inside the beating heart given in Table I, and the diameter of each of the designated inlets, we chose the averaged inlet coolant velocities of 1 m/s for the systemic circulation and 0.4 m/s for the pulmonary circulation using the UW coolant as the fluid. The outlet pressure values were assumed to be the same and equal to 101 kPa and constant. The temperature of the cooling fluid at the inlet was set as the minimal allowable temperature for the cooled organ, +4°C.

The same temperature boundary conditions as in the first scenario were applied on the cooling container walls. Although the lowest allowed temperature was set at +4°C in the simulations to avoid water ice crystals, some coolants with high osmolarities, such as UW solution, have a freezing point well below +4°C. A sub-zero temperature of the coolant would allow simulation of even faster cooling. However, it would likely not have a positive effect to enhance temperature uniformity in the heart wall, where temperature change is governed by heat conduction. A parallel computer with the Red Hat Enterprise Linux Server 6.2 OS and LSF scheduler was used for simulations. Thermofluid simulation was run on 4 Intel Xeon CPU E5-2420 processors. Each processor has 6 physical cores, 12 threads and 48 GB memory. Total computing time was 114,018 s.

Figure 4a illustrates the heart tissue's temperature distribution at the very beginning of the cooling process when the heart temperature was +37°C. The green color on the outermost surface of the heart is the initial coupled temperature between the warm heart and cold gelatin. This initial interface temperature was set as the average temperature of the heart and gelatin, which is +20.5°C. figures 4b to 3f demonstrate the heart cooling process. A constant color legend from +1°C to +37°C was used to better illustrate the temperature variation of the heart tissue. The red color in Figure 4b signifies the initial hot spots within the heart tissue. As the cooling process continued, the red color turned to green, and then blue due to the temperature reduction of the heart tissue. Therefore, the minimum and maximum temperatures of the heart are not necessarily equal to the minimal to maximal range of the color legend.

Figures 5a and 5b demonstrate the distribution of heart tissue's temperature at 300 s for two different cut-away views. Figure 5a reveals a large hot spot located above the right ventricle and on the right side of the right atrium.

Table VI. Boundary conditions for fluid domains.

Boundary Condition	**Heart Pulmonary Circulation**	**Heart Systemic Circulation**
Inlet velocity magnitude	0.4 m/s	1 m/s
Outlet pressure	101 kPa	101 kPa
Inlet coolant temperature	+4°C	+4°C

DOI: 10.1002/cnm

Figure 5b discloses two more hot spots; one is located on the left side of the left ventricle and the other is located on the right side of the left atrium.

Figure 6a shows the heart submersed in cooling gelatin without coolant flow at the beginning of cooling. Figures 6b to 6f illustrate the temperature distributions of the coolant flowing within the

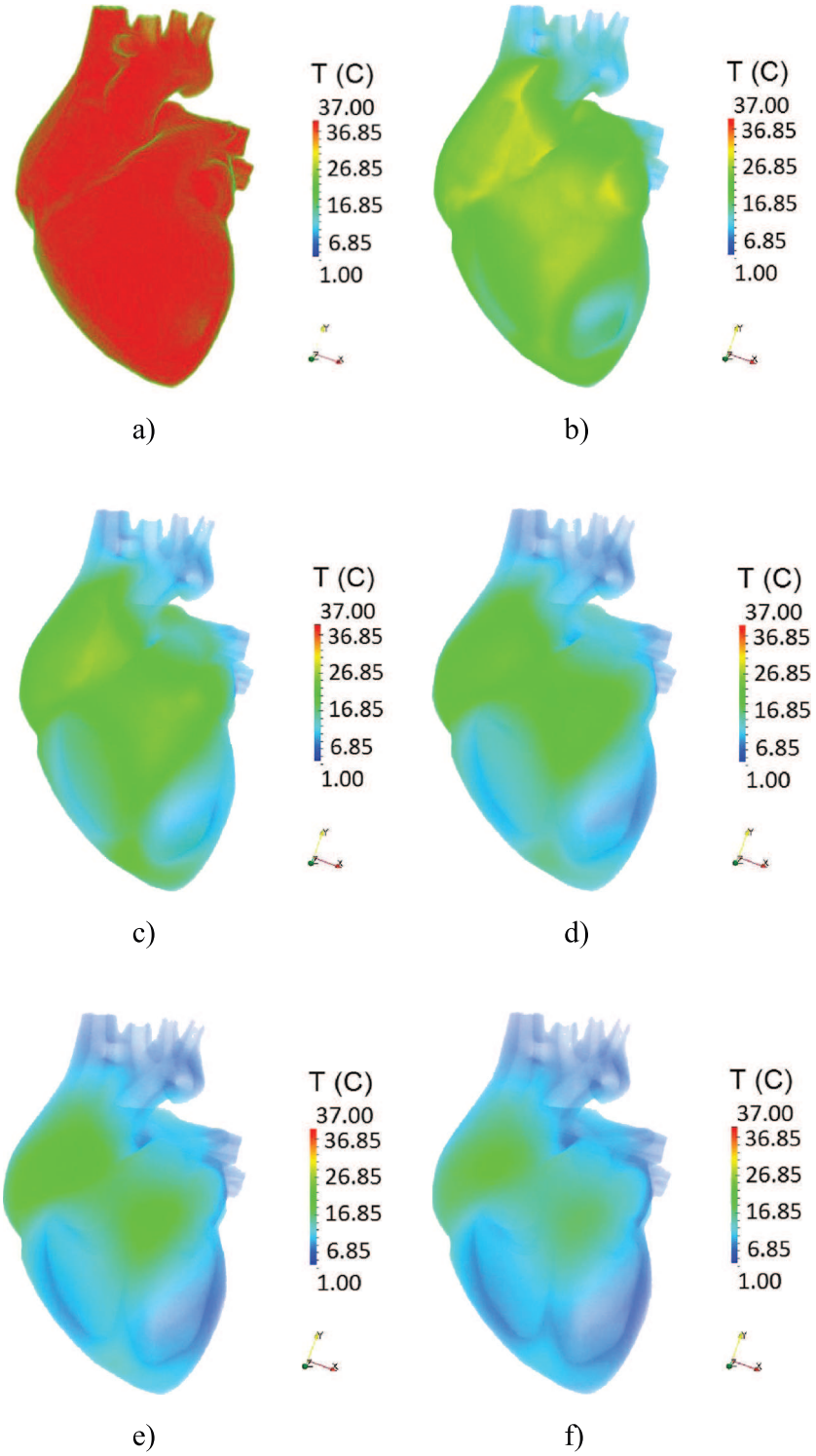

Figure 4. Temperature distribution of the heart tissue with constant color legend at times: a) 0 s, b) 300 s, c) 600 s, d) 900 s, e) 1200 s, and f) 1500 s.

DOI: 10.1002/cnm

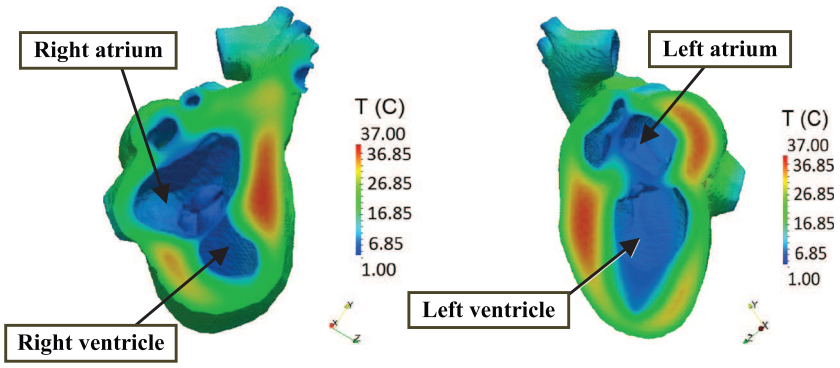

Figure 5. Temperature distribution at 300 s: a) 1st cut-away view, b) 2nd cut-away view.

heart as well as temperature distributions within the heart tissue and the surrounding gelatin. The minimum temperature in figures 6a to Figure 6f is -1°C, which is the minimum temperature of the cooling container walls. The temperature in this volume of the heart tissue was reduced from +37.0°C to a minimum of +15.8°C after 1500 s. Figure 6 gives a better understanding of temperature fields in one particular sagittal cut of the cooling system. The temperature on the other side of the cut will be identical (please note the color bar temperature distribution is the same).

To further reveal the temperature variations inside the heart during the cooling process, the maximum and minimum and average volumetric temperatures are shown in Figure 7a demonstrating that variation of the minimum temperature was not significant. The heart temperature began to decrease as soon as the coolant began to flow. Since the coolant inlet temperature was constant and the gelatin had its minimum temperature at the beginning of cooling, the minimum temperature of the heart did not change noticeably over time. The minimum temperature of the heart was +2.8°C after 1500 s of cooling, which is less than the target of +4°C. This low temperature occured on the very small part of outermost surfaces of the heart, which lay close to the container wall. The reason for this local low temperature is the small gap between the container wall, at -1°C, and the heart. At the same time, the maximum temperature was decreased by 18.9°C, that is, from +37.0°C to +18.1°C. The average volumetric temperature of the whole heart was calculated and is shown in Figure 7a. The minimum average volumetric temperature was reduced by 29.0°C, that is, from +37.0°C to +8.0°C after 1500 s. The coefficient of variation (*CV*) of temperature was used to study the temperature non-uniformity inside the heart. *CV* was defined as the ratio of standard deviation (*SD*) over the average value (T_{ave}) of temperature of the heart surface, where N is the number of grid cells in the heart tissue.

$$CV = \frac{SD}{T_{ave}} \tag{2}$$

$$SD = \sqrt{\frac{1}{N}\sum_{i=1}^{N}(T_i - T_{ave})^2} \tag{3}$$

$$T_{ave} = \frac{1}{N}\sum_{i=1}^{N} T_i \tag{4}$$

CV of the average volumetric temperature (Figure 7b) demonstrates that non-uniformity of the average volumetric temperature increased until 260 s and then started to decrease thus reducing the non-uniformity 2.23 times compared to its maximum.

Figure 8 illustrates temperature fields and the flow streamlines inside the heart pulmonary and systemic circulatory domains at 300 s. The maximum averaged coolant velocity occured in the pulmonary circulatory domain, just behind the semilunar valve, and was 2.13 m/s.

DOI: 10.1002/cnm

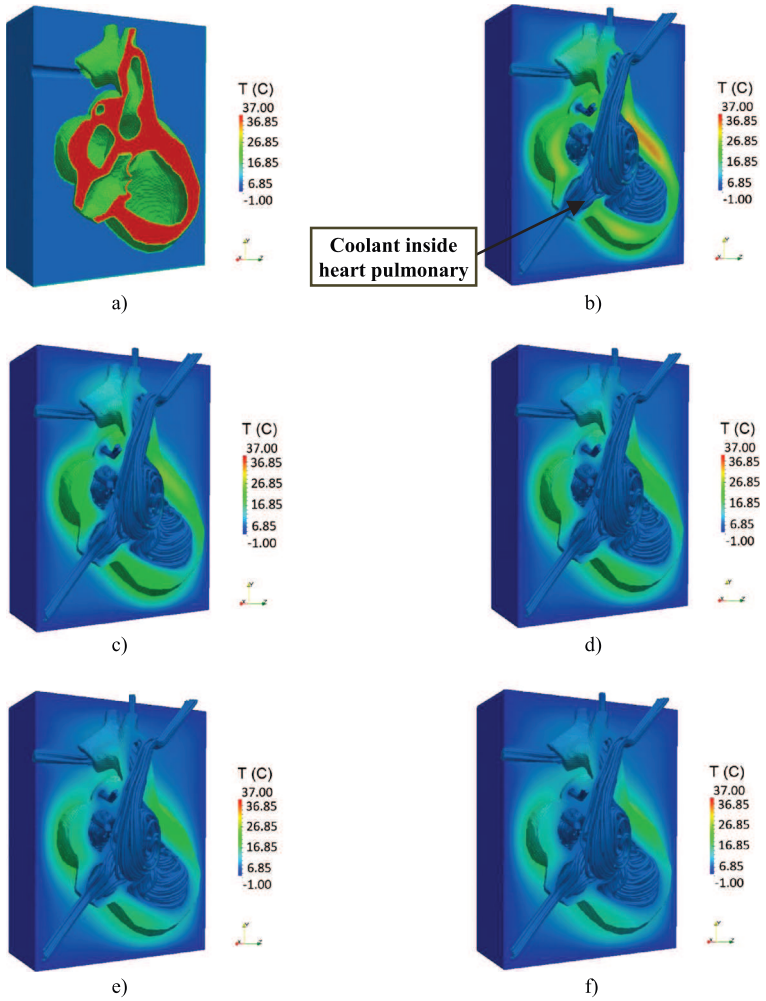

Figure 6. Temperature distribution (sagittal view) at times: a) 0 s, b) 300 s, c) 600 s, d) 900 s, e) 1200 s, and f) 1500 s.

Inlet flow rates can be determined from the averaged velocities at the inlets and diameters of the inlets. The flow rates for the two pulmonary circulatory inlets were calculated as 4826 ml/min and 4241 ml/min; for the two systemic circulatory inlets the values were 1086 ml/min and 271 ml/min. As Figure 8 shows, the temperature difference between the coolant and heart surfaces which were in

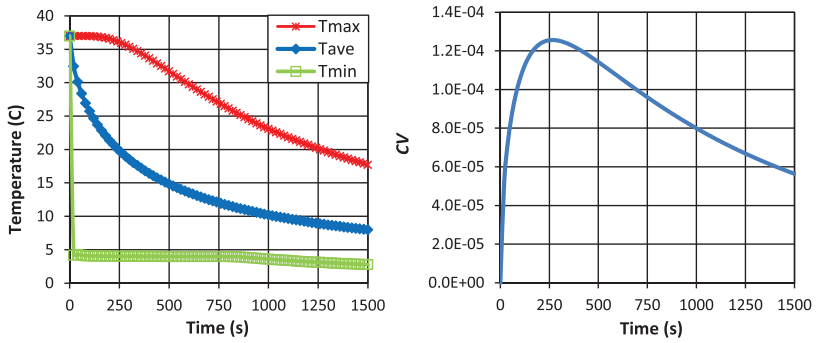

Figure 7. a) Temperature variations (maximum, minimum and average volumetric temperatures of the heart *vs*. time), and b) coefficient of variation of volumetric temperature *vs*. time.

DOI: 10.1002/cnm

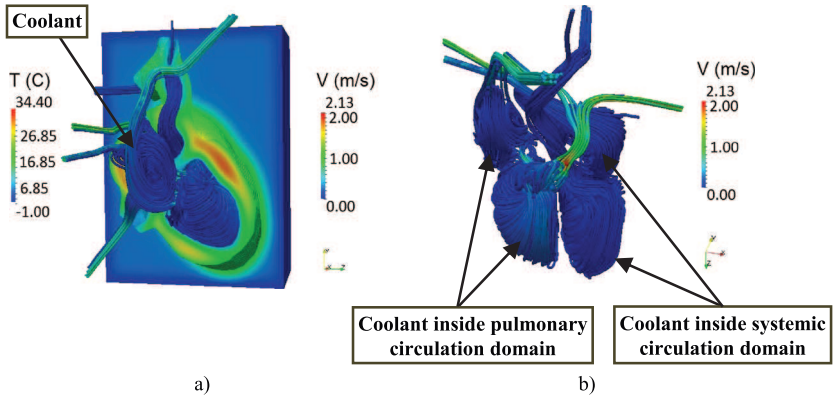

Figure 8. Coolant velocity distribution at 300 s: a) coolant inside the ventricles with temperature distribution inside the heart tissue and gelatin (cut-away view), and b) coolant velocity within the pulmonary and systemic circulatory domains.

contact with it, was almost zero. For discussion purposes only, let us analyse the heat convection law given as

$$q_{conv} = h_{conv} A \left(T_s - T_f\right) \tag{5}$$

where h_{conv} is the convection heat transfer coefficient, A is the contact surface area between fluid and solid. By increasing the flow rates (velocities), h_{conv} will increase. However, in this case since $(T_s - T_f)$ tends to zero, the h_{conv} effects will be almost negligible. Thus, increasing the coolant flow rates (velocities), would not only be ineffective in increasing the cooling rate, but would also increase the shear stresses on the heart-coolant interface, and possibly cause endothelial tissue damage. In the next step, the stress analysis was performed by using the data obtained from the thermo-fluid analysis results. A zero displacement assumption was applied for the heart's outermost surfaces. Normal and shear forces applied by the coolant flowing to the innermost surfaces were used as the boundary condition of these surfaces. These values were updated for each time step. The heart temperature field was used to obtain the thermal stresses during the cooling process.

As Table III shows, the ultimate tensile stress of cardiac muscle is 110 kPa. After obtaining the stress field measurement inside the heart, the maximum von Mises stress was calculated and is shown in Figure 9a. As this figure demonstrates, the maximum value of von Mises stress was almost constant (~96 kPa). Therefore, the effect of thermal stresses was not significant due to the

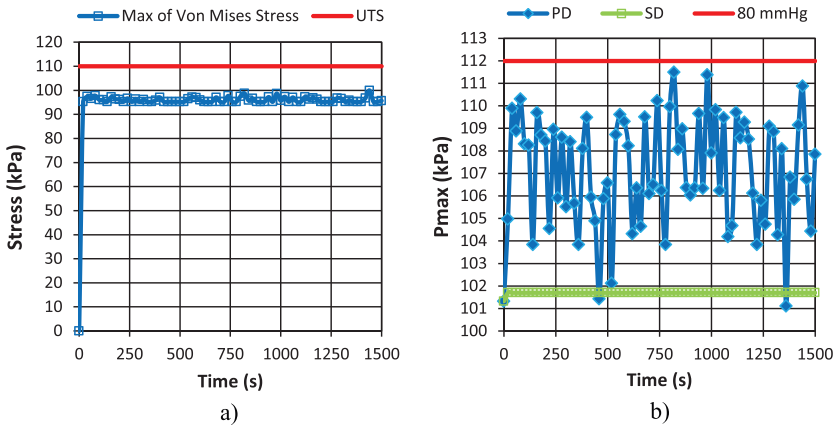

Figure 9. Maximum stress and pressure: a) maximum von Mises stress inside the heart tissue and ultimate tensile stresses *vs*. time, and b) maximum coolant pressure inside the pulmonary domain (PD) and systemic domain (SD).

DOI: 10.1002/cnm

very small Young's elastic modulus and thermal expansion coefficient of the heart tissue. Thus, only the forces caused by the flowing coolant played a major role in the stress field.

Figure 9b shows the maximum pressures of the coolant flowing within the pulmonary and systemic circulatory domains, including the heart chambers and major inlet and outlet vessels at every 20 s. Pressure distributions within the pulmonary and systemic circulatory domains are related to the velocity fields within these domains. In this model, the fluid flow was considered and simulated as an unsteady flow mainly because of the unsteady temperature field. Therefore, the velocity field (flow pattern) changed with time even though the inlet velocity was a constant value. This caused variations in the pressure field with time. Inside the pulmonary circulatory domain, the maximum pressure fluctuated with time, but inside the systemic circulatory domain the maximum pressure was almost a constant (~102 kPa). This was because within the pulmonary circulatory domain the velocity field variation with time was negligible. As a result, the pressure field variation with time was also negligible. However, as Figure 9b shows, the coolant velocity field within the pulmonary circulatory domain had larger values and larger variations. Therefore, this led to fluctuations in the pressure field as shown in Figure 9b. The purpose of this analysis was to estimate the maximum pressure that could occur within the heart during the cooling process. The importance of these simulations was to show that maximum pressures within the pulmonary and systemic circulatory domains remained less than 112 kPa (~80 mmHg).

It should be also mentioned that 80 mmHg which is the safe valve pressure for the systemic circulation is actually the total pressure behind the valve. This is usually considered the pressure within the right ventricle. The results showed that for systemic circulation the maximum pressure was much less than the 80 mmHg, so as the average pressure behind the valve. The total pressure in the pulmonary circulation was approximately 35 mmHg.

To further investigate shear stresses caused by the UW solution flows, heart wall shear stress (WSS) on the coolant-heart contact surfaces is plotted in Figure 10. Figure 10a demonstrates that on most of the coolant-heart contact surfaces, WSS was very small due to very small velocity gradients. The maximum WSS was 9.2 Pa which occurred in the pulmonary circulation domain at the pulmonary valve tip. The red oval in Figure 10a depicts the high WSS region. Figure 10b shows an enlarged cut-away view of the WSS distribution in this region. Higher WSS can also be observed at the inlet and outlet connections.

Accurate measurement of WSS applied on the entire liquid contact surfaces of the heart is very challenging. In one of the earliest research, Fry [29] showed that WSS higher than 40 Pa could damage the endothelial cell layer. Later, Moore *et al*. [30] reported that the maximum WSS on any artery in the normal cardiovascular system is expected to be less than 10 Pa. Oshinski *et al*. [31] applied MR phase velocity mapping to determine WSS in the aorta. They reported 5.4 Pa for the peak of wall shear stress in the aorta. Feldman *et al*. [32] reported that WSS of more than 7 Pa could produce endothelial damages in coronary arteries. Computationally predicted WSS results presented in the present study showed that in most parts of the heart-liquid contact surface, WSS was lower than 2 Pa. The maximum WSS at the pulmonary valve tip is also

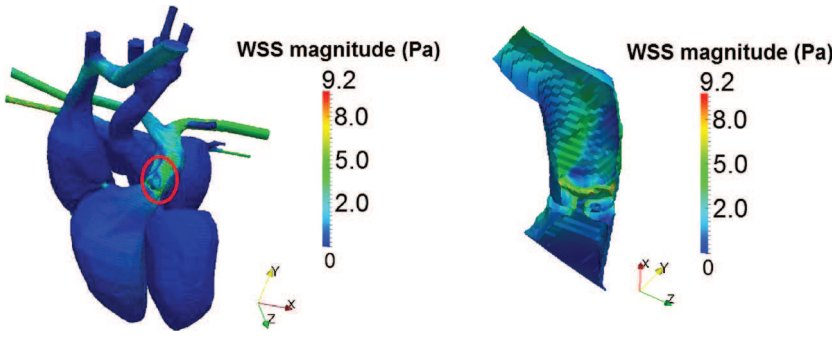

a) b)

Figure 10. Wall shear stress magnitude: a) entire heart-liquid contact surface, and b) cut-away enlarged view of higher shear stress region.

DOI: 10.1002/cnm

expected to be lower in the real case since it will open more due to the fluid pressure. Therefore, the large velocity gradient at its tip will reduce. However, one can apply a constrained optimization algorithm (Colaco and Dulikravich [33]) to find the maximum coolant flow rate at which WSS will be kept below its safe limit value.

3.3. Computational grid independency

Accuracy of the computational results depends on the size of the average computational grid cells. Dependency of the simulations was studied by comparing computational results obtained on two different grids. Figure 11 illustrates the heart hexahedral grid used for simulations presented in this paper and results obtained on a finer heart grid to examine the grid dependency of the simulations.

The finer computational grid information for each domain is presented in Table VII. The total number of grid cells for all domains was 10,900,000. Table VIII shows the simulation results (at 20 s) obtained by using the first grid having 4,200,000 grid cells with details given in Table IV

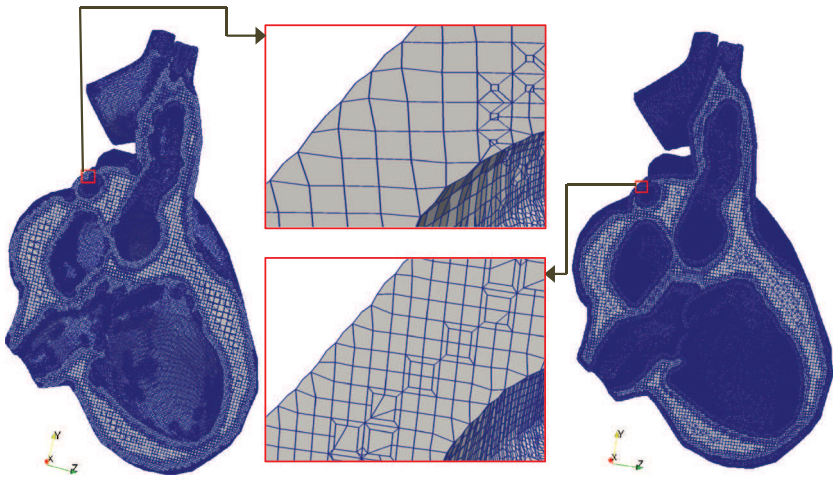

Figure 11. Heart computational grid: a) used for simulations presented in this paper, and b) finer grid used for comparative simulation until 20 s.

Table VII. Finer hexahedral grid cells for different computational domains.

Domain	**Number of grid cells**
Heart pulmonary circulation	~ 1,200,000
Heart systemic circulation	~ 1,200,000
Heart	~ 5,000,000
Gelatin	~ 3,500,000

Table VIII. Comparison of simulation results for two computational grids at 20 s.

Parameter	**Case 1**	**Case 2**	**Variation**
Total number of grid cells	~ 4,200,000	~ 10,900,000	~ +6,700,000
Minimum temperature (°C)	+4.0	+4.0	0
Maximum temperature (°C)	+37	+37	0
Average volumetric temperature (°C)	+32.40	+32.46	+0.06
Maximum von Mises stress (kPa)	95.248	95.154	-0.094
WSS (Pa)	9.243	9.290	+0.047
Computation time (s)	1,496.24	15,482.12	+13,985.88

DOI: 10.1002/cnm

(case 1). Case 2 in Table VIII presents the simulation results obtained by applying the finer grid. Variations between case 1 and case 2 results are also shown in this table. As these results show, results of case 2 were in good agreement with results of case 1. However, the computation time in case 2 was 13986 s more than the computation time in case 1 for these 20 seconds of simulated cooling process.

4. CONCLUSIONS

A 3-D thermo-fluids-stress combined computational analysis was performed using high resolution, realistic human heart geometry during 1500 s of a cooling process. Using OpenFOAM software platform to perform all numerical simulations, it was shown that the average volumetric temperature of the heart decreased by 29°C after 1500 s of cooling when pumping a liquid solution at +4°C. Therefore, based on the Q_{10} law, the metabolic rate would have been reduced by 93% in this case. The temperature non-uniformity of the heart tissue was increasing until 260 s of cooling, and then it began to decrease as the cooling continued. The variation of minimum temperature of the heart was negligible, while the maximum temperature decreased by 18.9°C during 1500 s of cooling. It was also demonstrated that cooling only with gelatin from the outside was not sufficient to cool the inner parts of the heart wall within the desired time interval. Stress analysis results showed that the maximum von Mises stress inside the heart was less than the ultimate tensile stress of the cardiac muscle. The maximum pressures of the liquid solution pumped within the heart pulmonary and systemic circulatory domains were less than 80 mmHg. The maximum WSS was 9.2 Pa, which occurred in the pulmonary circulation domain at the pulmonary valve tip. Improving uniformity of temperature distribution in the heart tissue throughout the cooling process could be computationally explored via optimally controlled coolant jets instead of gelatin in the space between the heart and the cooling container. A future objective is to incorporate an even more detailed realistic human heart geometry which includes coronary arteries and apply multi-objective optimization methods to the cooling analyses presented in this report that will optimize the cooling rate and uniformity, while decreasing shear stresses at the coolant-heart tissue interface.

ACKNOWLEDGEMENTS

The authors also gratefully acknowledge the FIU Instructional and Research Computing Center for providing HPC resources in conducting this project. The research of Chandrajit Bajaj was supported in part by NIH grant R01-EB004873.

REFERENCES

1. Wagner FM. Donor heart preservation and perfusion. *Applied Cardiopulmonary Pathophysiology* 2011; **15**:198–206.
2. Reyes AB, Pendergast JS, Yamazaki S. Mammalian peripheral circadian oscillators are temperature compensated. *Journal of Biological Rhythms* 2008; **23**:95–98.
3. Moore EM, Nichol AD, Bernard SA, Bellomo R. Therapeutic hypothermia: benefits, mechanisms and potential clinical applications in neurological, cardiac and kidney injury. *International Journal care Injured* 2011; **42**(9):843–854.
4. Polderman KH, Herold I. Mechanisms of action, physiological effects, and complications of hypothermia. *Critical Care Medicine* 2009; **37**:S186–202.
5. Stowe DF, Heisner JS, An JZ, Camara AKS, Varadarajan SG, Novalija E, Chen Q, Schelling P. Inhibition of Na^+/H^+ exchange-1 isoform protects hearts reperfused after six hour cardioplegic cold storage. *Journal Of Heart And Lung Transplantation* 2002; **21**:374–382.
6. Jahania MS, Sanchez JA, Narayan P, Lasley RD, Mentzer RM. Heart preservation for transplantation: principles and strategies. *Annals of Thoracic Surgery* 1999; **68**:1983–1987.
7. Dulikravich GS. Inverse design and active control concepts in strong unsteady heat conduction. *Applied Mechanics Reviews* 1988; **41**(6):270–277.
8. Dennis BH, Dulikravich GS. Determination of unsteady container temperatures during freezing of three-dimensional organs with constrained thermal stresses. *International Symposium on Inverse Problems in Engineering Mechanics – ISIP'2k*, Tanaka M, Dulikravich GS (eds.). Nagano, Japan, *Elsevier Science Ltd*, Amsterdam, 2000; 139–148.

DOI: 10.1002/cnm

9. Sterk M, Trobec R. Biomedical simulation of heat transfer in a human heart. *Journal of Chemical Information and Modeling* 2005; **45**:1558–1563.
10. Webster JG. *Medical instrumentation application and design, chapter 7: blood pressure and sound*, (4th edn), Peura R (ed.). John Wiley & Sons, Hoboken, NJ, 2009; ISBN-10: 0471676004.
11. Wexler L, Bergel DH, Gabe IT, Makin GS, Mills CJ. Velocity of blood flow in normal human venae cavae. *Cardiovascular Research, Circulation Research* 1968; **23**(3):349–359.
12. Gisvold SE, Brubakk AO. Measurement of instantaneous blood-flow velocity in the human aorta using pulsed Doppler ultrasound. *Cardiovascular Research* 1982; **16**(1):26–33.
13. Zhang Y, Bajaj C. Finite element meshing for cardiac analysis. *ICES Technical Report 04-26*, 2004; University of Texas at Austin.
14. Bajaj C, Goswami S. Modeling cardiovascular anatomy from patient-specific imaging. *Advances in Computational Vision and Medical Image Processing*, Tavares J, Jorge R (ed.). Springer, chapter 1, 2008; 1–28, NIHMS155076.
15. Southard JH, Belzer FO. Organ preservation. *Annual Review of Medicine* 1995; **46**:235–247.
16. Arunachalam BK, Millard RW, Kazmierczak MJ, Rodriguez-Rilo HL, Banerjee PK. Evaluation of thermal efficacy of hypothermic tissue preservation methods. *Cell Preservation Technology* 2006; **4**:97–116.
17. Freitas Jr RA. Nanomedicine, volume I: basic capabilities. Publisher: *Landes Bio-science*, 1999; ISBN-13: 978-1570596803.
18. Kisslo JA, Adams BD. Principles of Doppler echocardiography and the Doppler examination #1. London: *Ciba-geigy*, 1987.
19. Stein PD, Sabbah HN. Turbulent blood flow in the ascending aorta of humans with normal and diseased aortic valves. *Circulation Research* 1976; **39**:58–65.
20. OpenCFD Ltd. OpenFOAM. <http://www.opencfd.co.uk /openfoam/>, 2000-2013.
21. Ferziger JH, Peric M. Computational methods for fluid dynamics. *Springer*, *3rd edition*, 2001.
22. Ohayon J, Chadwick RS. Effects of collagen microstructure on the mechanics of the left ventricle. *Biophysical Journal* 1988; **54**(6):1077–1088.
23. Yamada H. *Strength of biological materials*. Evans FG (ed.), Williams & Wilkins: Baltimore, MD, 1970; ISBN-13: 978-0683093230.
24. Park J, Lakes RS. Biomaterials: an introduction. *Springer*; *3rd edition*, 2007; ISBN-13: 978-0387378794.
25. Amini AA, Prince JL. Measurement of cardiac deformations from MRI: physical and mathematical models. *Springer*, *1st edition*, 2001; ISBN-13: 978-1402002229.
26. Palmeri ML, Nightingale KR. On the thermal effects associated with radiation force imaging of soft tissue. *IEEE Transactions on Ultrasonics, Ferroelectrics, and Frequency Control* 2004; **51**(5):551–565.
27. Hou G, Wang J, Layton A. Numerical methods for fluid-structure interaction— a review. *Communications in Computational Physics* 2012; **12**:337–377.
28. Peltola J, Pättikangas T, Brockmann T, Siikonen T, Toppila T, Brandt T. Adaptation and validation of OpenFOAM®CFD-solvers for nuclear safety related flow simulations. *SAFIR* 2010; 17.5., CSC, Espoo, Finland, 2011.
29. Fry DL. Acute vascular endothelial changes associated with increased blood velocity gradients. *Circulation Research* 1968; **22**:165–197.
30. Moore JE Jr, Xu C, Glagov S, Zarins CK, Ku DN. Fluid wall shear stress measurements in a model of the human abdominal aorta: oscillatory behavior and relationship to atherosclerosis. *Atherosclerosis* 1994; **110**(2):225–240.
31. Oshinski JN, Ku DN, Mukundan S Jr, Loth F, Pettigrew RI. Determination of wall shear stress in the aorta with the use of MR phase velocity mapping. *Journal of Magnetic Resonance Imaging* 1995; **6**:640–71995.
32. Feldman CL, Ilegbusi OJ, Hu Z, Nesto R, Waxman S, Stone PH. Determination of *in vivo* velocity and endothelial shear stress patterns with phasic flow in human coronary arteries: A methodology to predict progression of coronary atherosclerosis. *American Heart Journal* 2002; **143**(6):931–939.
33. Colaço JM, Dulikravich GS. A survey of basic deterministic, heuristic and hybrid methods for single-objective optimization and response surface generation. *Chapter 10 in Thermal Measurements and Inverse Techniques*, Orlande HRB, Fudym O, Maillet D, Cotta R (eds.). CRC Press: Boca Raton, FL, 2011; 355–405.

DOI: 10.1002/cnm